IEEE Access
Multidisciplinary | Rapid Review | Open Access Journal

Received January 17, 2020, accepted January 31, 2020, date of publication February 4, 2020, date of current version February 12, 2020.

Digital Object Identifier 10.1109/ACCESS.2020.2971538

Zero Guard Band Multi-Twin-SSB System in Single Fiber Bidirectional PON Transmission

XIANG GAO, YUANCHENG CAI, BO XU, FAITH KWAKU DEYNU, AND KUN QIU
Key Laboratory of Optical Fiber Sensing and Communications, Ministry of Education, University of Electronic Science and Technology of China, Chengdu 611731, China

Corresponding author: Bo Xu (xubo@uestc.edu.cn)

ABSTRACT We propose a novel zero guard band (ZGB) multi-twin-SSB bidirectional passive optical network system which combines the multiband carrier-less amplitude phase and twin single sideband (SSB) modulation techniques. The multi-twin-SSB signal is generated at the downlink transmitter side with zero guard band between the left-sideband and right-sideband. A weak local oscillator which is extracted from the uplink optical source aids the downstream signal detection. Kramers-Kronig algorithm is used at both downlink and uplink receiver sides to reconstruct the SSB signal and eliminate the signal-signal beat interference. The downstream and upstream signals are transmitted in a single fiber without any spectral overlap between them and the Rayleigh backscattering noise is removed by the optical band-pass filter. The proposed scheme is extensively investigated and analyzed with four sub-bands using 50 Gbps 16-QAM modulation for each sub-band over a bidirectional 50 km transmission. The results show that, compared with the conventional multi-twin-SSB scheme, the proposed ZGB multi-twin-SSB scheme can improve the spectral efficiency by about 11%. The required optical signal to noise ratio (OSNR) and the required received optical power (ROP) can be reduced by more than 15 dB and 7 dB respectively at the 7% hard decision forward error correction (HD-FEC) threshold (bit error rate of 3.8×10^{-3}), respectively. For the uplink transmission, the required ROPs for the inner and outer sub-bands at 7% HD-FEC are about −10 dBm and −11 dBm, respectively. And the signal to noise ratio to the corresponding ROPs for the inner and outer sub-bands are 15.4 dB and 15.3 dB, respectively.

INDEX TERMS Passive optical network, twin single sideband, Rayleigh backscattering, Kramers-Kronig.

I. INTRODUCTION

With the continuous growing number of network users and the emergence of new network business applications such as live-streaming of high definition video multimedia and cloud computing using remote data storage, the potential capacity demand imposes challenging burdens on passive optical networks (PONs) [1]–[10]. To improve the capacity of optical transmission systems, a variety of advanced modulation formats have been proposed, including subcarrier modulation (SCM) [11], [12], orthogonal frequency division multiplexing (OFDM) [13], [14] and carrier-less amplitude phase (CAP) modulation [15]. The conventional SCM needs electrical mixer and radio frequency source which makes the architecture complex. Some of previous works have been demonstrated the feasibility for the application of OFDM in PON system [16], [17], but the OFDM has a high peak-to-average power ratio which makes its performance sensitive to the transceiver devices. The multiband CAP (multi-CAP) was proposed in Ref. [18] which breaks a single-band signal into multiple sub-bands in order to tailor the modulation order depending on the signal to noise ratio (SNR) in each sub-band. The multi-CAP technique can reach high data rate by using different modulation formats and components with limited bandwidth and less complexity. Hence, the CAP modulation with multiband has been considered as a promising low cost solution for the multiple-user PON systems and has attracted extensive investigations [18]–[21]. In 2013, Miguel Iglesias *et al*. experimentally demonstrated 102 Gbps transmission over 15 km fiber with 6 sub-bands multi-CAP [18]. The modulation formats for each sub-band were 36 ary quadrature amplitude (QAM) for the first three sub-bands, 16-QAM for the next two bands, and 4-QAM for the last band. In the same year,

The associate editor coordinating the review of this manuscript and approving it for publication was Qunbi Zhuge.

Junwen Zhang *et al.* verified a wavelength division multiplexing (WDM) CAP-PON architecture based on multi-CAP 16-QAM with 5 sub-bands [19]. In 2019, Youxu Zen *et al.* successfully demonstrated a 6 sub-bands CAP-WDM-PON scheme with 5 wavelengths over 20 km fiber transmission based on the discrete multi-tone (DMT) and Hilbert transformed single sideband (SSB) modulation [21]. In brief, the multi-CAP technique can provide large capacity with the flexibility and elasticity of the modulation formats.

To combat the power fading induced by fiber chromatic dispersion (CD) and improve the spectral efficiency (SE) of WDM systems, SSB modulation has been proposed and triggered intensive discussions [22]–[32]. However, there are two serious shortcomings about the conventional SSB system: one is that the signal-signal beat interference (SSBI) induced by the square-law detection of the photodiode (PD) significantly degrades the system performance; and the other is that the partial bandwidth of the transmitter digital-to-analog converters (DACs) are wasted because the SSB signal only carries one sideband information. To overcome the SSBI effect, a guard band equal to the bandwidth of the SSB signal can be introduced between the optical carrier and information carrying sideband to make sure the spectra of the desired signal and the SSBI do not overlap [24]–[26]. Obviously, the SE will be almost halved. In 2016, Mecozzi *et al*. proposed a direct detection coherent receiver based on the Kramers-Kronig (KK) relations [27] which theoretically eliminated the SSBI by reconstructing the field of a linearly modulated SSB signal. Moreover, the KK based receiver not only overcomes the SSBI effect without guard band but also reduces the required carrier to signal power ratio (CSPR) before the square-law detection [28]–[32]. On the other hand, in order to make full use of the bandwidth of the DACs at the transmitter side, in 2015, Liang Zhang *et al*. proposed a novel modulation called twin-SSB technique in which two groups of independent signals were modulated onto the left-sideband (LSB) and the right-sideband (RSB), respectively [33]. A commercially available quadrature point biased dual driver Mach-Zehnder modulator (DDMZM) was used to generate the optical twin-SSB signal and a pair of optical band-pass filters (OBPFs) and PDs were employed for signal detection. This scheme has attracted significant interest in many areas of optical communications in recent years [34]–[42]. In 2017, Sunjie Fan *et al*. proposed a spectrally efficient twin-SSB system based on the time-interleaved OFDM and experimentally verified the scheme by 80 km fiber transmission with the bit rate of 88.3 Gbps [35]. In 2018, Gordon Ning Liu *et al*. reviewed the typical transmission techniques in the 5G fronthaul, data center interconnect and metro application, and concluded that the twin-SSB modulation could achieve a high SE in these systems [38]. However, one shortcoming still exists in the conventional twin-SSB scheme. A part of unwanted sideband remains at the other side of the optical carrier because of the non-ideal property of the OBPF. This residual unwanted sideband will beat with the desired sideband during the square-law detection resulting in interference that can hardly be eliminated. Therefore, a guard band needs to be introduced between the LSB and RSB signals at the transmitter side which will reduce the SE. Ref. [41] reduced the guard band by using multiple-input-multiple-output (MIMO) processing to equalize the crosstalk of the undesired sideband with an increased computation complexity. Ref. [42] used an asymmetric structure to remove the guard band of one sideband but the guard band of the other sideband still existed.

Rayleigh backscattering (RB) noise is also another obstacle for the bidirectional transmission. Lots of works have been done recently for RB noise mitigation [43]–[45]. Ref [43] used a radio frequency signal synthesizer to reduce the spectral overlap between the distributed carrier and desired signal. In this case, the RB noise was eliminated but the system became more complicated. Ref. [44], [45] introduced guard band between the downstream and upstream signals. The system performances were improved but the SE was reduced as well.

In this paper, we propose and investigate a novel zero guard band (ZGB) multi-twin-SSB bidirectional PON system which combines the multiband CAP and twin-SSB modulation techniques. At the downlink transmitter side, a null point biased IQ modulator is utilized to modulate a carrier-less optical ZGB multi-twin-SSB signal. At the receiver side, an OBPF and a weak optical local oscillator (LO) are used before detection. The weak LO is extracted from the uplink optical source with its central frequency laying at the edge of the downstream signal. For the uplink transmitter, the SSB modulation is applied with the spectra laying at the opposite side of the downstream signal. So that the RB noise is easily removed by the OBPF. The proposed ZGB multi-twin-SSB PON scheme is analyzed and verified by 50 Gbps 16-QAM signals with 4 sub-bands over 50 km bidirectional fiber transmission. Some key advantages of the proposed ZGB multi-twin-SSB scheme are listed as follow: 1) No guard band is needed between the LSB and RSB signals so the SE is higher than that of conventional twin-SSB scheme; 2) The required optical signal to noise ratio (OSNR) for the downlink transmission is reduced and the receiver sensitivity is improved due to the optical carrier suppressed transmission and the heterodyne detection; 3) The SSBI is eliminated and the required optical LO power from the uplink laser is reduced because of the application of the KK algorithm. 4) The RB noise is easily eliminated since the upstream and downstream signals are at different sides of the optical carrier.

This is an extension of our previous work published in [46]. Compared to [46], we present in this paper a novel scheme to further improve the SE for the downlink transmission, and verify the scheme by theoretical analyses and numerical simulations.

II. PRINCIPLE OF THE ZGB MULTI-TWIN-SSB PON

The schematic architecture of the ZGB multi-twin-SSB bidirectional PON is shown in Fig. 1. At the optical line terminal (OLT) side, a continuous-wave laser with central frequency of f_d is used as the optical source for the

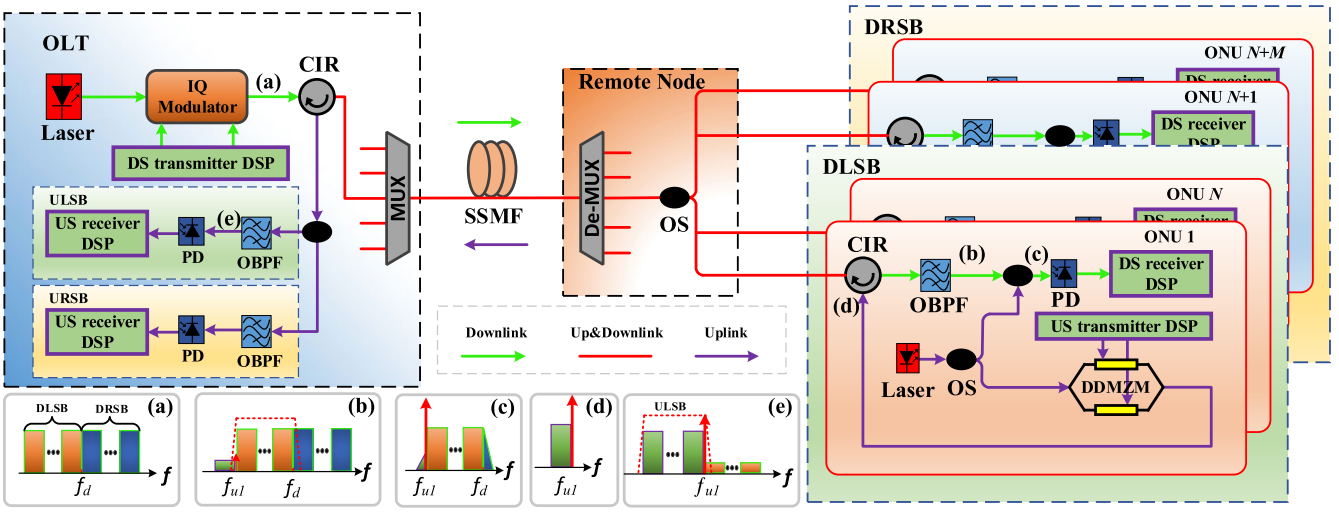

FIGURE 1. Schematic of single fiber multi-twin-SSB bidirectional PON architecture. Insets: (a) spectrum of the IQ modulator output at the optical line terminal (OLT) side which includes the downstream left side-band (DLSB) and downstream right side-band (DRSB) signals. (b) Spectrum of the DLSB signal after an optical band-pass filter (OBPF). (c) Spectrum of the DLSB signal after coupling with the optical local oscillator (LO). (d) Spectrum of the ONU1 uplink signal. (e) Spectrum of the upstream left side-band (ULSB) signal after an OBPF. DS, downstream; US, upstream; CIR, optical circulator; MUX, multiplexer; OS, optical splitter; PD, photodiode; f_d, central frequency of downlink light source; f_{u1}, central frequency of ULSB signal uplink light source.

downlink transmission. The multi-twin-SSB signal is generated at the transmitter side digital signal processing (DSP) using shaping filters (SFs) and Hilbert transform filters according to Ref. [46] but with zero guard between the downstream LSB (DLSB) and downstream RSB (DRSB) signals. For the n-th sub-band, the impulse response of two root-raised-cosine (RRC) based orthogonal SFs are given by [19]

$$SF_I^n(t) = g(t)\cos[\pi(2n-1)(1+\beta)Rs\cdot t], \quad (1)$$

$$SF_Q^n(t) = g(t)\sin[\pi(2n-1)(1+\beta)Rs\cdot t], \quad (2)$$

$$g(t) = \frac{\sin[\pi(1-\beta)Rs\cdot t] + 4\beta Rs\cdot t\cos[\pi(1+\beta)Rs\cdot t]}{\pi Rs\cdot t\left[1-(4\beta Rs\cdot t)^2\right]}, \quad (3)$$

where, β is the roll off factor, Rs is the symbol rate which is also the reciprocal of the symbol time period. Two groups of multi-CAP signals which combined with N and M sub-bands respectively can be express as

$$s_{CAP1}(t) = \sum_{i=1}^{N}\left[SF_I^i(t)\otimes s_I^i(t) - SF_Q^i(t)\otimes s_Q^i(t)\right], \quad (4)$$

$$s_{CAP2}(t) = \sum_{k=1}^{M}\left[SF_I^k(t)\otimes s_I^k(t) - SF_Q^k(t)\otimes s_Q^k(t)\right], \quad (5)$$

where, $\otimes$ represents the convolution operation, $s_I^x(t)$ and $s_Q^x(t)$ are the I and Q data after QAM mapping and up-sampling for the x-th sub-band, respectively. Then a pair of Hilbert transform filters are applied to $s_{CAP1}(t)$ and $s_{CAP2}(t)$ to generate the multi-twin-SSB signal which is expressed as

$$s_{twin}(t) = \underbrace{s_{CAP1}(t) - jH[s_{CAP1}(t)]}_{DLSB} + \underbrace{s_{CAP2}(t) + jH[s_{CAP2}(t)]}_{DRSB}, \quad (6)$$

where $H[x]$ represents Hilbert transform. Note that no guard band is necessary between the DLSB and DRSB signals during the above multi-twin-SSB generation process. In order to clearly demonstrate the principle of the multi-twin-SSB transmission, in the following, the summed DLSB signals will be treated as one integrated signal that obtained from a complex baseband signal $s_{bl}(t)$ with $-B_{DLSB}/2$ frequency shifting where B_{DLSB} represents the optical bandwidth of the DLSB signals. The DRSB signal is defined similarly using $s_{br}(t)$ with $B_{DRSB}/2$ frequency shifting. The multi-twin-SSB signal can be rewritten as

$$s_{twin}(t) = s_{bl}(t)\exp(-j\pi B_{DLSB}t) + s_{br}(t)\exp(j\pi B_{DRSB}t). \quad (7)$$

A null point biased optical IQ modulator is used to convert the modulated signal into optical domain with the optical carrier suppressed. For simplicity, the IQ modulator is assumed as an ideal linear modulator and the optical multi-twin-SSB signal can be expressed as $s_{twin}(t)\exp(j2\pi f_d t)$. The spectrum of the optical downstream signal is shown in the inset (a) of Fig. 1. After an optical circulator, the modulated optical downstream signal is launched into a standard single-mode fiber (SSMF) and transmitted towards the optical network units (ONUs). Multiple wavelengths can be applied in the WDM transmission system where each wavelength carries a multi-twin-SSB signal. We chose only one of the wavelengths to demonstrate this scheme for simplicity. At the remote node, the optical signal is firstly split by a de-multiplexer for different users. Then, an OBPF is applied after an optical circulator to remove the crosstalk of the undesired sideband and the RB noise from the upstream signal. The filtered DLSB and DRSB signal can be expressed as

$$s_{DLSB}(t) = s_{bl}(t)\exp\left[j2\pi\left(f_d - \frac{B_{DLSB}}{2}\right)t\right], \quad (8)$$

$$s_{DRSB}(t) = s_{br}(t)\exp\left[j2\pi\left(f_d + \frac{B_{DRSB}}{2}\right)t\right]. \quad (9)$$

In practice, there will be a residual part from the undesired side band because of the non-ideal property of the OBPF. But the residual part will not affect the performance of the receiver for the proposed scheme. Detailed discussion of this effect is carried out in part B of this Section. The inset (b) of Fig. 1 shows the spectrum of the DLSB signal and the principle the OBPF filtering. At the ONU side, the filtered signal is coupled with a weak optical LO which is extracted from the light source of the uplink transmitter. The central frequencies of the uplink lasers are set to $f_{u1} = f_d - B_{DLSB}$ and $f_{u2} = f_d + B_{DRSB}$ for the DLSB and DRSB group users, respectively. The inset (c) of Fig. 1 shows the spectrum of DLSB signal after coupled with the optical LO. Then the filtered optical SSB signal is detected by a single-ended PD. The square-law detection can be modeled as

$$\begin{aligned} I_{DLSB}(t) &= \left|\begin{array}{l} A_l\exp\left[j2\pi\left(f_d - B_{DLSB}\right)t\right] \\ +s_{bl}(t)\exp\left[j2\pi\left(f_d - \frac{B_{DLSB}}{2}\right)t\right]\end{array}\right|^2 \\ &= \left|A_l + s_{bl}(t)\exp\left(j\pi B_{DLSB}t\right)\right|^2, \quad (10) \\ I_{DRSB}(t) &= \left|\begin{array}{l} A_r\exp\left[j2\pi\left(f_d + B_{DRSB}\right)t\right] \\ +s_{br}(t)\exp\left[j2\pi\left(f_d + \frac{B_{DRSB}}{2}\right)t\right]\end{array}\right|^2 \\ &= \left|A_r + s_{br}(t)\exp\left(-j\pi B_{DRSB}t\right)\right|^2, \quad (11) \end{aligned}$$

where, A_l and A_r are the amplitudes of the optical LO for the DLSB and DRSB signals, respectively. According to (10) and (11), the filtered DLSB and DRSB signals after coupled with the optical LOs can be regarded as RSB and LSB signals, respectively. If the detected signal satisfied the minimum phase condition, the KK algorithm [27] can be applied for the SSB signal reconstruction as

$$\phi_{DLSB}(t) = \frac{1}{2\pi}p.v.\int_{-\infty}^{+\infty}dt'\frac{\ln\left[I_{DLSB}(t')\right]}{t-t'}, \quad (12)$$

$$\phi_{DRSB}(t) = \frac{1}{2\pi}p.v.\int_{-\infty}^{+\infty}dt'\frac{\ln\left[I_{DRSB}(t')\right]}{t-t'}, \quad (13)$$

$$\begin{aligned} s_{bl}(t) &= \left\{\sqrt{I_{DLSB}(t)}\exp\left[j\phi_{DLSB}(t)\right] - A_l\right\} \\ &\quad\times\exp\left(-j\pi B_{DLSB}t\right), \quad (14) \\ s_{br}(t) &= conj\left\{\sqrt{I_{DRSB}(t)}\exp\left[j\phi_{DRSB}(t)\right] - A_r\right\} \\ &\quad\times\exp\left(j\pi B_{DRSB}t\right), \quad (15) \end{aligned}$$

where *p.v.* denotes the Cauchy principal value of the integral. After the KK algorithm, the data of each sub-band can be recovered by using a matched filter (MF) which is similar to the conventional multi-CAP technique [19].

For cost consideration, only a single DDMZM is utilized at the uplink transmitter. LSB and RSB modulations are applied to the DLSB and DRSB group users respectively to ensure that the spectra of the upstream and downstream signals do not overlap. After SSMF transmission, an OBPF is used before the single-ended PD and the signal is then processed by the DSP. Details of the DSP for both downlink and uplink transmitter and receiver are carried out in Section 3. The spectrum of the upstream LSB (ULSB) after the SSMF transmission and the principle the OBPF filtering is shown in the inset (e) of Fig. 1. Obviously, the downstream and upstream signals are located at different sides of the optical carrier, so the RB noise can be easily removed by the OBPF before PD detection.

In this scheme, although an optical LO is necessary for heterodyne detection of the downstream signal, the light is extracted from the uplink transmit laser. So, the cost of this scheme does not increase much compared with PON systems where optical sources exist in both OLT and ONU sides. The uplink transmitter uses part of its light source power in exchange for the improvement of the SE and performance for the downlink transmission. Fortunately, the KK algorithm can greatly reduce this distributary power because required CSPR for the KK receiver is much lower than the conventional receiver.

A. THE IQ MODULATOR BASED MULTI-TWIN-SSB SCHEME

In the proposed ZGB multi-twin-SSB PON downlink transmission, a null point biased IQ modulator is applied instead of the conventional quadrature point biased DDMZM [23], [37], [38] or an IQ modulator biased above the null point [39], [42]. As widely known, the DDMZM working at push-pull mode can be modeled with two parallel phase modulators and the output of the DDMZM can be expressed as [47]

$$\begin{aligned} &E_{out}(t) \\ &= \frac{1}{2}E_{in}\left[\exp\left(j\pi\frac{s_1(t)+V_{b1}}{V_\pi}\right) + \exp\left(j\pi\frac{s_2(t)+V_{b2}}{V_\pi}\right)\right] \\ &= \frac{1}{2}E_{in}\left\{\begin{array}{l}\cos\left(\pi\frac{s_1(t)+V_{b1}}{V_\pi}\right)+\cos\left(\pi\frac{s_2(t)+V_{b2}}{V_\pi}\right) \\ +j\left[\sin\left(\pi\frac{s_1(t)+V_{b1}}{V_\pi}\right)+\sin\left(\pi\frac{s_2(t)+V_{b2}}{V_\pi}\right)\right]\end{array}\right\} \\ &= CE_{in}\cos\left[\frac{\pi}{2V_\pi}\Delta V_b + \frac{\pi}{V_\pi}s(t)\right], \quad (16) \\ &P_{out}(t) \\ &= \left|E_{out}(t)\right|^2 \\ &= \frac{1}{2}P_{in}\left\{1+\cos\left[\frac{\pi}{V_\pi}\Delta V_b + 2\frac{\pi}{V_\pi}s(t)\right]\right\}, \quad (17) \end{aligned}$$

where E_{in} represents the input optical field, V_{b1} and V_{b2} are the direct current (DC) bias voltages for the upper and lower branches, $s_1(t)$ and $s_2(t)$ are the radio frequency signals, respectively. And for the push-pull mode, $s_1(t) = -s_2(t) = s(t)$. V_π is the half-wave voltage parameter of the MZM, $C = \exp[j\pi(V_{b1} + V_{b2})/(2V_\pi)]$, which is a constant phase shift, $\Delta V_b = V_{b1} - V_{b2}$, P_{out} and P_{in} are the output and input optical power, respectively.

At the null point of the DDMZM (where $\Delta V_b = V_\pi$), the Taylor series expansion with respect to $s(t)$ can be derived from (16) and given by

$$\begin{aligned} E_{out}(t) &= CE_{in}\cos\left[\frac{\pi}{2}+\frac{\pi}{V_\pi}s(t)\right] \\ &= -CE_{in}\sin\left[\frac{\pi}{V_\pi}s(t)\right] \\ &= -CE_{in}\left[\frac{\pi}{V_\pi}s(t)-\frac{1}{3!}\left(\frac{\pi}{V_\pi}s(t)\right)^3+\cdots\right]. \end{aligned} \quad (18)$$

The first term is the linearly modulated signal and the other terms are the high order disturbances. While, at the quadrature point of the DDMZM (where $\Delta V_b = V_\pi/2$), the Taylor series expansion with respect to $s(t)$ is given by

$$\begin{aligned} E_{out}(t) &= CE_{in}\cos\left[\frac{\pi}{4}+\frac{\pi}{V_\pi}s(t)\right] \\ &= -\frac{\sqrt{2}}{2}CE_{in}\left[\sin\left(\frac{\pi}{V_\pi}s(t)\right)-\cos\left(\frac{\pi}{V_\pi}s(t)\right)\right] \\ &= -\frac{\sqrt{2}}{2}CE_{in}\left[-1+\frac{\pi}{V_\pi}s(t)+\frac{1}{2!}\left(\frac{\pi}{V_\pi}s(t)\right)^2\right. \\ &\quad \left.-\frac{1}{3!}\left(\frac{\pi}{V_\pi}s(t)\right)^3+\cdots\right]. \end{aligned} \quad (19)$$

If the terms above 3-rd order are ignored, it can be observed from (19) that both 2-nd and 3-rd order nonlinear terms exist when the DDMZM is biased at the quadrature point. In contrast, the equation (18) shows that only 3-rd order nonlinear term exists when the DDMZM is biased at the null point. Typically, the term $\pi s(t)/V_\pi$ is usually kept less than 1 by adjusting the optical modulation index (OMI) [48]. In this case, the higher the order of a term means the less power it takes. For this reason, with the same OMI, the DDMZM working at its null point suffers less nonlinear disturbance compared with that working at the quadrature point. For comparison, the typical transmission curve of the DDMZM is shown in Fig. 2. It can be observed that the null point locates the best field-wise linearity where the output field E_{out} can be approximately considered as a linear representation of the input field E_{in}. While at the quadrature point of the DDMZM, the output power P_{out} can be approximately considered as a linear representation of the input power P_{in}. Accordingly, the quadrature point biased DDMZM is usually used as an intensity modulator in short-reach communications [19], [20]. Therefore, the null point biased IQ modulator which consists of two DDMZMs can produce more linear modulation compared with the quadrature point biased single DDMZM with the same OMI [48]–[50]. Furthermore, since the optical carrier is not transmitted with the signal, the proposed IQ modulator based scheme can also improve the receiver sensitivity and reduce the required OSNR of the downlink transmission.

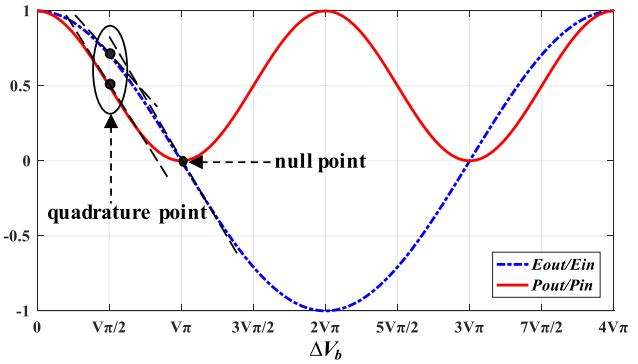

FIGURE 2. Typical transmission curve for the DDMZM.

B. THE SSBI AT THE ONU SIDE

Figure 3 (I) and (II) show the schematics for the conventional DDMZM based twin-SSB downlink transmission and the proposed IQ modulator based twin-SSB downlink transmission. For simplicity, only the DLSB signal receiving process is considered for explaining the principle. In the conventional scheme, the DDMZM needs to be biased at its quadrature point to generate the optical twin-SSB signal with an optical carrier as shown in the inset (a) of Fig. 3 (I). An OBPF is needed at the receiver side to obtain an optical SSB signal. Because of the non-ideal property of the OBPF, a part of the undesired sideband will still exist before detection as shown in the inset (b) of Fig. 3 (I). Hence, the square-law detection can be typically modeled as

$$\begin{aligned} I_1(t) &= |A + s_{lsb}(t)\exp(-j2\pi f_1 t) + s_{res}(t)\exp(j2\pi f_2 t)|^2 \\ &= A^2 + 2As_{lsb}(t)\cos(j2\pi f_1 t) + 2As_{res}(t)\cos(j2\pi f_2 t) \\ &\quad + 2As^*_{lsb}(t)\,s_{res}(t)\cos[j2\pi(f_1+f_2)t] \\ &\quad + |s_{lsb}(t)|^2 + |s_{res}(t)|^2, \end{aligned} \quad (20)$$

where, A represents the optical carrier amplitude, $s_{lsb}(t)$ donates the desired LSB signal, $s_{res}(t)$ is the residual part of the RSB signal after the OBPF, f_1 and f_2 are the central frequencies of $s_{lsb}(t)$ and $s_{res}(t)$ respectively, $*$ denotes the complex conjugate. According to (20), since $s_{lsb}(t)$ and $s_{res}(t)$ are at different sides of the optical carrier, the desired LSB signal (the second term) suffers from four kinds of crosstalk: the residual part crosstalk (the third term), the desired sideband signal with the residual part signal beat interference (the fourth term), the desired sideband SSBI (the fifth term), and the residual part SSBI (the sixth term). The corresponding electrical spectrum after square-law detection is shown in the inset (c) of Fig. 3 (I). Because the optical signal before square-law detection is no longer a SSB signal, the phase information is destroyed and can hardly be reconstructed by the DSP. Therefore, a guard band need to be introduced between the LSB and RSB signals at the transmitter side, which will limit the SE. In the proposed ZGB twin-SSB downlink transmission, the IQ modulator is biased at its null point to suppress the optical carrier before launching into the fiber as shown by the spectrum in the inset (d) of Fig. 3 (II). At the receiver side, the optical signal is also filtered by an

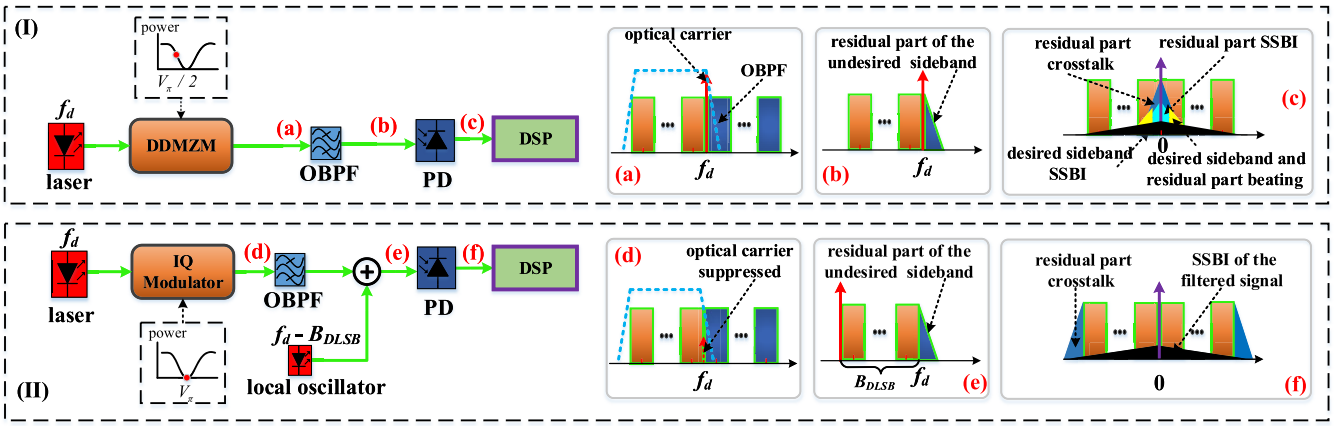

FIGURE 3. Schematic architectures for conventional DDMZM based downlink scheme (I) and the proposed IQ modulator based downlink scheme (II). Inset (a)-(c) represent the LSB signal spectra before OBPF, after OBPF and after PD detection for the conventional DDMZM based scheme; Inset (d)-(f) represent the LSB signal spectra before OBPF, after coupling with the optical LO, and after PD detection respectively for the proposed IQ modulator based scheme.

OBPF and then coupled with an optical LO whose center frequency is set to the left edge of the filtered sideband as depicted by the spectrum in the inset (e) of Fig. 3 (II). For simplicity, the following square-law detection can be modeled as

$$\begin{aligned} I_2(t) &= |A + [s_{lsb}(t) + s_{res}(t)] \exp(j2\pi ft)|^2 \\ &= A^2 + 2A[s_{lsb}(t) + s_{res}(t)] \cos(j2\pi ft) \\ &\quad + |s_{lsb}(t) + s_{res}(t)|^2, \end{aligned} \tag{21}$$

where f represents the central frequency of $s_{lsb}(t) + s_{res}(t)$. In this case, the residual part of the undesired sideband and the desired sideband are at the same side of the LO with non-overlapping spectra. Hence they can be regarded as an integrated SSB signal as shown in the inset (e) of Fig. 3. For this reason, the SSBI of the whole filtered signal can be easily eliminated by KK algorithm. Moreover, since the spectra of the residual part crosstalk and the desired signal do not overlap, the residual part crosstalk also can also be removed by a corresponding MF. The spectrum after square-law detection is shown in the inset (f) of Fig. 3 (II). Furthermore, since the required CSPR of KK receiver is much lower than the conventional gapless receiver, only a weak LO (which can be extracted from the uplink light source) is required to reconstruct the SSB signal. It should be noted that, as two unrelated lasers are applied in this process, the phase noise will appear in the desired signal. Fortunately, this kind of noise can be easily compensated by some classic phase estimation algorithms [51]–[53] after the SSB field reconstruction by the KK receiver. Therefore, no guard band is needed in the proposed twin-SSB scheme.

C. SPECTRA ALLOCATION FOR DOWNLINK AND UPLINK

Figure 4 shows the spectra allocation for the downstream signal (a) and the upstream signal (b) of the proposed ZGB multi-twin-SSB bidirectional PON system. For downlink transmission, the multi-twin-SSB is modulated without guard band and the sub-bands are divided into DLSB and

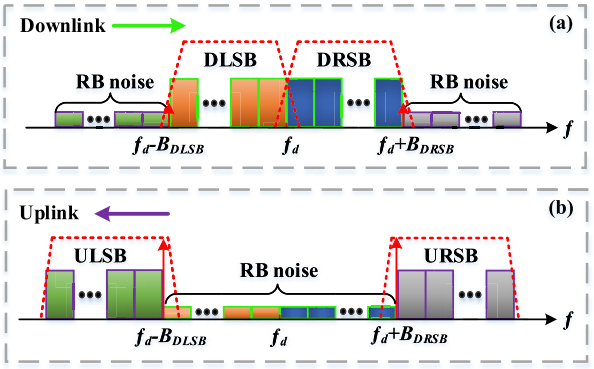

FIGURE 4. Spectra of the downstream signal (a) and the upstream signal (b) for the proposed ZGB multi-twin-SSB bidirectional PON transmission system. RB, Rayleigh backscattering.

DRSB groups. At the receiver side, the users in different groups are filtered out by different OBPFs before PD detection. The optical LOs are located at left and right edges of the spectra for the DLSB and DRSB signals, respectively. For uplink transmission, LSB and RSB modulations are applied for the users in the DLSB and DRSB groups, respectively. Note that the SSB modulation applied in both downlink and uplink transmission can help the PON system against the power fading induced by the CD of fiber. As a single fiber is used for bidirectional transmission, the RB noise will occur and degrade the system performance. However, the spectra for the downstream and upstream signals are at different sides of the optical carrier and the amplitude of the RB noise is much lower than the desired signal. So, the RB noise for both downlink and uplink can be easily removed by the OBPF.

III. SIMULATION VERIFICATION AND RESULTS DISCUSSION

In order to validate the proposed ZGB multi-twin-SSB bidirectional PON scheme, numerical simulations were conducted using the Virtual Photonics Incorporated

Transmission Maker 9.1 integrated with Matrix Laboratory (MATLAB). The simulated system followed the schematic of Fig. 1 with some simplifications. For downlink transmission, two sub-bands of LSB were assumed for ONU1 and ONU2 and the other two sub-bands of RSB for ONU3 and ONU4. The transmitter side DSP function is shown in Fig. 5 (a). A pseudo random binary sequence (PRBS) with 2^{18} bits was used for each sub-band with the symbol rate $Rs = 12.5$ Gbaud. For simplicity, all of the sub-bands were modulated with the modulation format of 16-QAM. After 8 times up-sampling, the signals were digitally shaped by root-raised-cosine (RRC) filter with a roll-off factor of $\beta = 0.1$. Then a pair of digital Hilbert transform filters were applied to obtain the SSB signals located in the LSB and RSB, respectively. The central frequencies of ONU1-ONU4 were set to $f_1 = -3Rs(1+\beta)/2, f_2 = -Rs(1+\beta)/2, f_3 = Rs(1+\beta)/2$ and $f_4 = 3\ Rs(1+\beta)/2$, respectively. The spectrum of the electrical downstream signal is shown in the inset (I) of Fig. 5 (a). The generated electrical signal was then fed into an optical IQ modulator which was biased at its null point. A laser source with 200 kHz linewidth and frequency of $f_d = 193.1$ THz was used as downstream optical source. A SSMF with a length of 50 km and attenuation coefficient of 0.2 dB/km was assumed in this work. Other parameters of the SSMF included dispersion coefficient D of 16 ps/nm/km, and non-linear index of $2.6 \times 10^{-20} \mathrm{m}^2/\mathrm{W}$. A 4-th order Gaussian filter was applied to model the OBPF at the receiver side while its 3 dB bandwidth was set to $B_w = 2\ Rs(1+\beta)$ to obtain the desired sideband signal. The filtered LSB and RSB optical signals were coupled with two kinds of optical LO with linewidth of 1-MHz whose central frequencies were set to $f_{u1} = f_d - 2\ Rs(1+\beta)$ and $f_{u2} = f_d + 2\ Rs(1+\beta)$, respectively. The optical SSB signals were detected by single-ended PDs. The responsivity and dark current of the PD for each ONU was set to 0.85 A/W and 0.5 nA, respectively. The induced SSBI after the square-law detection is shown in the insets of Fig. 5 (b). The obtained electrical signals were then processed by the MATLAB using the receiver side DSP function shown in Fig. 5 (b). KK algorithm was firstly applied to cancel the SSBI of the downstream signal. After that, digital CD compensation is conducted in the frequency domain and then the data stream corresponding to i-th ONU was digitally filtered by a MF. Note that as the central frequencies of the optical LOs locatedat the left and right edges of the LSB and RSB downstream signals, the location of the sideband of the received electrical signals were inverse of the transmitter side. Hence, the central frequencies of the ONU1-ONU4 at the receiver side were f_3, f_4, f_1 and f_2, respectively. The positions of the desired sub- bands in LSB and RSB signals is shown in the inset (II) and inset (III) of Fig. 5 (b), respectively. After digital filtering, the signal was down-sampled by 8 times followed by a phase noise compensation (PNC) processing [51]. Finally, the QAM signals were demodulated for bit error rate (BER) calculation.

For the uplink transmission, a quadrature point biased single DDMZM was applied to modulate SSB signal. The

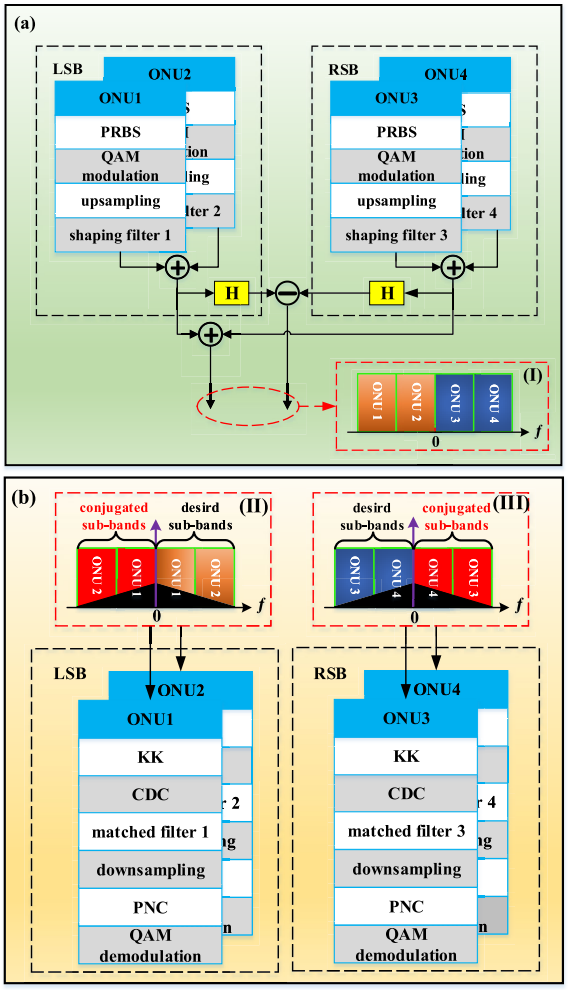

FIGURE 5. DSP structure of the downlink transmitter side (a) and receiver side (b). Inset: (I) spectrum of the downstream electrical signal; (II) spectrum of the LSB electrical signal after PD detection; (III) spectrum of the RSB electrical signal after PD detection. H: Hilbert transform.

DSP functions at the uplink transmitter and receiver sides are shown in Fig. 6 (a) and (b). For the upstream operation, the data for different users were modulated by 16-QAM format and digitally filtered by SFs with a Hilbert transform filter. The symbol rate, RRC roll-off factor and the central frequencies of ONU1-ONU4 were the same as the down-stream signals. At the receiver side, the optical signals were filtered by two OBPFs whose central frequencies located at $f_{u1} - Rs(1+\beta)$ and $f_{u2} + Rs(1+\beta)$ with 3 dB bandwidth of B_w for the ULSB and URSB group users respectively, and then detected by single-ended PDs. The operation for the uplink receiver side DSP was almost the same as downlink. Since the optical carrier was transmitted together with the signal and they exhibit the same phase noise, no PNC was needed in the receiver side DSP.

A. OPTIMAL CSPR

The KK algorithm can reconstruct the field of a linearly modulated SSB signal and effectively eliminate the SSBI

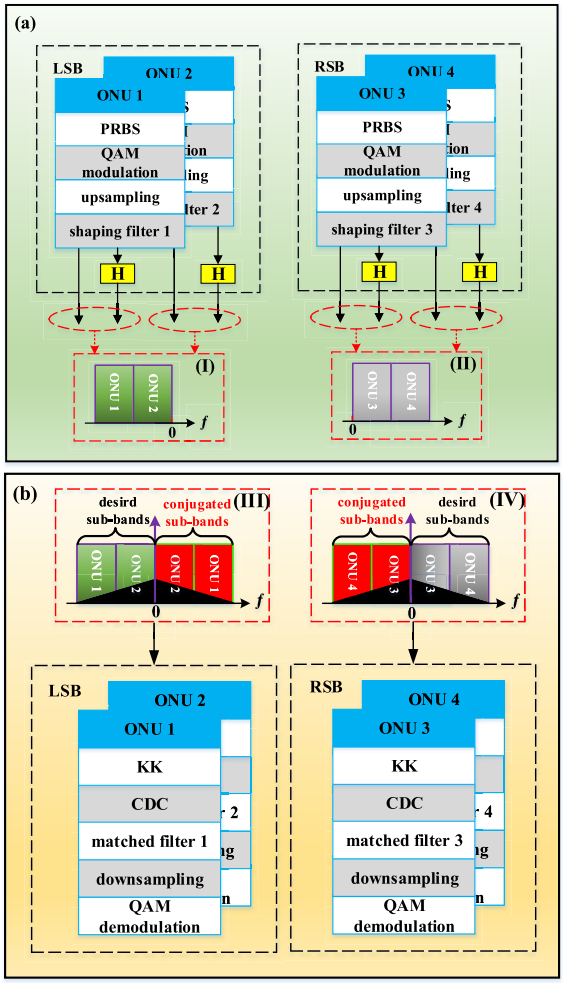

FIGURE 6. DSP structure of the uplink transmitter side (a) and receiver side (b). Inset: (I) spectrum of the transmitter upstream LSB electrical signal; (II) spectrum of the transmitter upstream RSB electrical signal; (III) spectrum of the LSB electrical signal after PD detection; (IV) spectrum of the RSB electrical signal after PD detection.

induced by the square-law detection when the minimum phase condition is satisfied [27]. Compared with the conventional receiver, KK receiver can remarkably reduce the required CSPR and significantly improve the performance with no guard band introduced between the optical carrier and the desired sideband signal [28]–[30]. To investigate the required CSPR of the proposed scheme, Fig. 7 shows the SNR performance of the ZGB multi-twin-SSB for all sub-bands as a function of CSPR after 50 km fiber transmission at the OSNR of 35 dB and the total detected optical power remains constant at 0 dBm. The SNR is calculated before the QAM signal demodulation and defined as $\mathrm{SNR(dB)} = -20\log_{10}(\mathrm{EVM})$ according to Ref. [54], where EVM is the error vector magnitude of the received signal. The total detected optical power P_{total} and the CSPR are defined as

$$P_{total} = P_{LO} + P_{sig}, \tag{22}$$

$$\mathrm{CSPR(dB)} = 10\log_{10}\left(\frac{P_{LO}}{P_{sig}}\right), \tag{23}$$

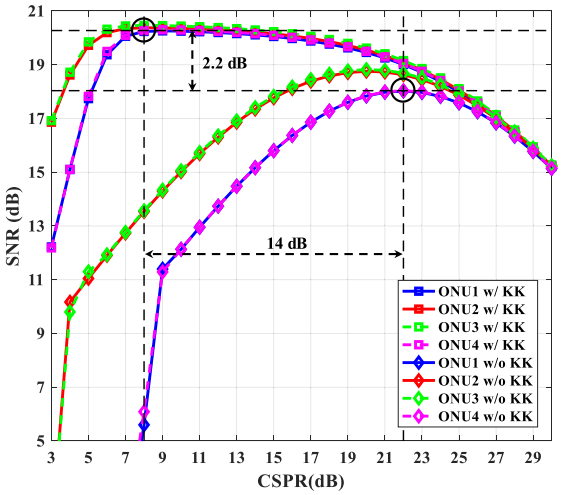

FIGURE 7. SNR performance versus CSPR for the conventional receiver and the KK receiver after 50 km downlink transmission at the OSNR of 35 dB and the total detected optical power remains at 0 dBm.

where P_{LO} is the power of the optical LO which is extracted from the light source of the uplink transmitter, P_{sig} is the received optical signal power (ROP) which contains the filtered optical SSB signal only. It should be noted that the CSPR is varied by adjusting P_{LO} and P_{sig} while keeping the total detected optical power P_{total} constant. When the CSPR is insufficient, the KK algorithm cannot reconstruct the SSB signal because the minimum phase condition is not satisfied [27]. So, the SNR performance increases with the CSPR until it reaches an optimal value (CSPR = 8 dB). It should be noted that, since the optical LOs lay at the left and right edges of the DLSB and DRSB signals, respectively. According to (10) and (11), the filtered DLSB and DRSB signals after coupled with the optical LOs can be regarded as RSB and LSB signals, respectively. Hence, the ONU1 and ONU4 are considered as the inner sub-bands while ONU2 and ONU3 are the outer sub-bands. As shown in the insets (II) and (III) of the Fig.5 (b), since the SSBI has a triangular spectrum in the frequency domain, the inner sub-bands (ONU1 and ONU4) suffer stronger SSBI than that of outer sub-bands (ONU2 and ONU3). So, the performances of ONU1 and ONU4 decrease more rapidly compared to ONU2 and ONU3 as the CSPR goes below 8 dB. When the CSPR is larger than 8 dB, the KK algorithm can work well under the minimum phase condition. In this case, the performances of inner sub-bands are almost equal to those of outer sub-bands. Since the total detected optical power P_{total} is kept constant, the signal power P_{sig} keeps decreasing as the CSPR grows. The shot and thermal noises of the PD become the major limitation of the receiver in this case. So, the system performance begins to deteriorate when the CSPR keeps growing. Finally, when the CSPR is larger than 25 dB, P_{LO} is approximately equal to 0 dBm, and the P_{sig} is very weak. Hence, $\mathrm{CSPR(dB)} \approx 0 - 10\log_{10}(P_{sig})$, and the SNR can be expressed as $\mathrm{SNR(dB)} = 10\log_{10}(P_{sig}) - 10\log_{10}(P_{noise}) = -\mathrm{CSRP(dB)} - 10\log_{10}(P_{noise})$, where P_{noise} is the noise power of the receiver. Since P_{noise} remains constant, when the CSPR is larger than 25 dB, the SNR

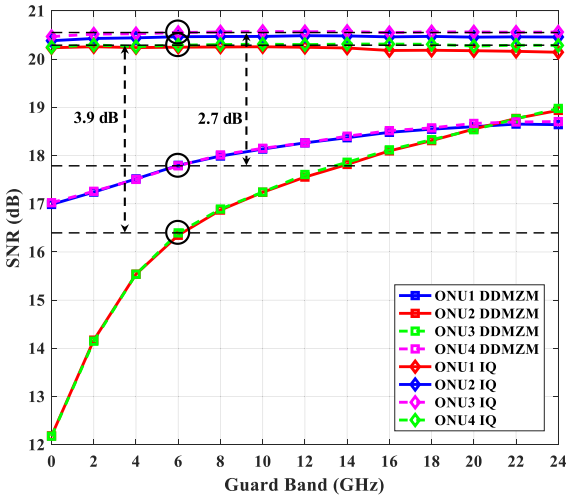

FIGURE 8. SNR performance versus guard band between LSB and RSB downstream signals for the conventional DDMZM based multi-twin-SSB scheme and the proposed IQ modulator based ZGB multi-twin-SSB scheme after 50 km downlink transmission at the OSNR of 35 dB and the ROP remains at 0 dBm.

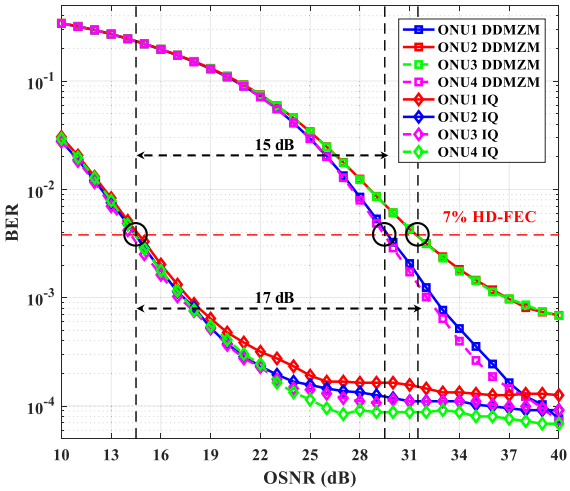

FIGURE 9. BER performance versus OSNR for the conventional DDMZM based multi-twin-SSB scheme and the proposed IQ modulator based ZGB multi-twin-SSB scheme at the ROP of 0 dBm after 50 km downlink transmission.

almost shows a linear decline with the CSPR. For the conventional receiver without KK algorithm, the signal can hardly be demodulated when the CSPR is too low (i.e., CSPR $<$ 6 dB for inner sub-bands and CSPR $<$ 4 dB for outer sub-bands). The optimal CSPR for the conventional receiver is about 22 dB at the total detected optical power of 0 dBm. Therefore, the KK receiver can reduce the CSPR by about 14 dB. Because of the SSBI elimination feature, KK receiver can also improve the SNR performance by about 2.2 dB at the optimal CSPR. Therefore, thanks to the KK algorithm, the uplink laser only needs to extract a weak light for the downstream signal detection.

B. GUARD BAND

To investigate the SE improvement of the proposed downlink scheme, Fig. 8 shows the SNR performances of the

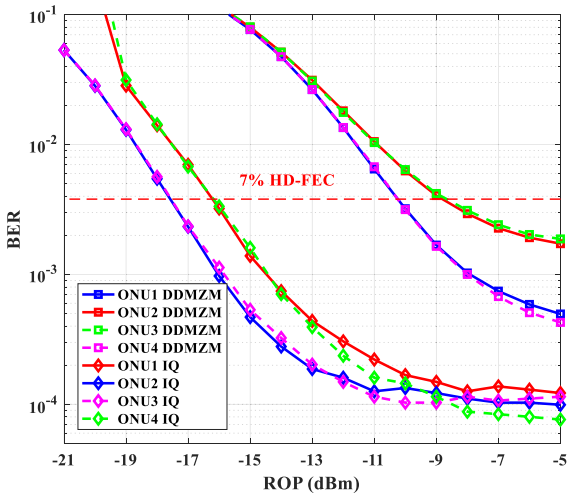

FIGURE 10. BER performance versus ROP for the conventional DDMZM based multi-twin-SSB scheme and the proposed IQ modulator based ZGB multi-twin-SSB scheme at the OSNR of 35 dB after 50 km downlink transmission.

conventional and the proposed ZGB multi-twin-SSB schemes versus guard band after 50 km downlink transmission at the OSNR of 35 dB while the ROP remains constant at 0 dBm. These results are obtained by KK receiver at the optimal CSPR with corresponding optimal OMI [46]. The guard band defined here is the bandwidth between the LSB and RSB signals. Note that, since the optical carrier for the conventional scheme is in the middle of the four sub-bands, ONU2 and ONU3 are considered as the inner sub-bands while ONU1 and ONU4 are the outer sub-bands. When the guard band is below 6 GHz, the SNR performances of the conventional scheme decrease rapidly because the residual part of the undesired sideband breaks the condition for the SSB signal reconstruction. For the proposed ZGB scheme, the performances for all the sub-bands are almost stable with the guard band increasing. This is because the whole filtered signal coupling with the optical LO can be regarded as an integrated SSB signal and this kind of SSBI is easily eliminated by KK algorithm as we discussed previously in Section. 2.2. Therefore, the proposed ZGB multi-twin-SSB scheme can help improving the SE by about 11%. Furthermore, as the null point is where the best field-wise linearity locates for the DDMZM, the proposed null point biased IQ modulator based ZGB scheme can improve the SNR performances by about 3.9 dB and 2.7 dB for inner and outer sub-bands respectively compared with the conventional DDMZM based scheme with a guard band of 6 GHz.

C. REQUIRED OSNR

As the optical carrier is not transmitted together with the modulated signal in the proposed scheme, the required OSNR is reduced compared with the conventional scheme because the optical carrier at the modulator output takes a large proportion of the power. To investigate this issue, Fig. 9 shows the BER performances for the conventional DDMZM based scheme and the proposed IQ modulator based ZGB scheme as

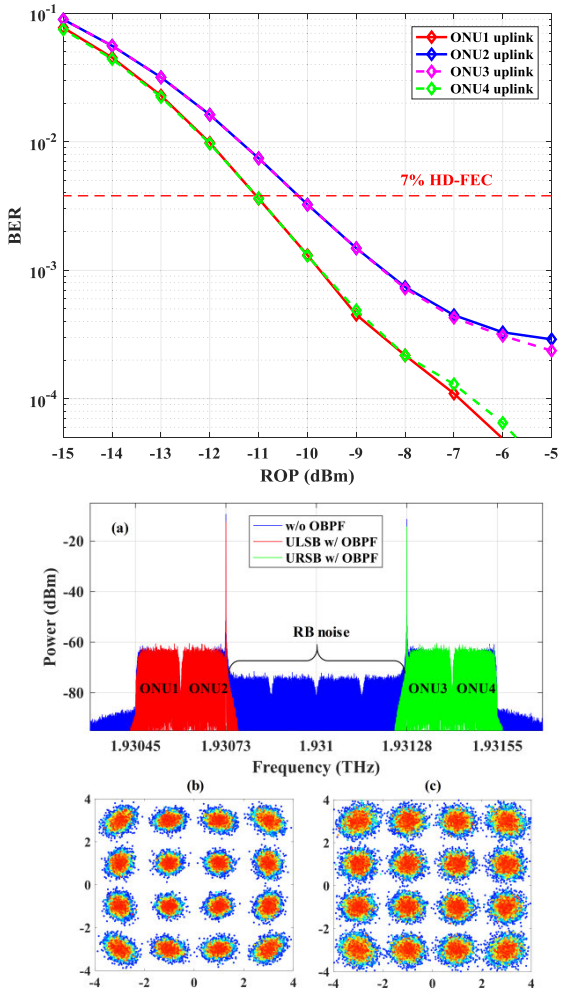

FIGURE 11. BER performance versus ROP at the OSNR of 35 dB after 50 km uplink transmission. Inset: (a) represents the spectra of the upstream signals; (b) and (c) represent the constellations of the ONU1 and ONU2 upstream signals at the ROP of −5 dBm, respectively.

a function of OSNR after 50 km fiber downlink transmission at the ROP of 0 dBm. The results for both of the schemes are obtained at the optimal parameters. The guard band of the conventional scheme is set to 6 GHz while no guard band is used for the proposed scheme. For the conventional scheme, it is observed a performance difference between the inner and outer sub- bands when the OSNR is larger than 28 dB due to the nonlinear effect of the quadrature point biased DDMZM and the residual unwanted sideband interference. The proposed ZGB multi-twin-SSB scheme can reduce the required OSNR by about 17dB and 15 dB at 7% hard decision forward error correction (HD-FEC) threshold (BER = 3.8×10^{-3}) for the inner and outer sub-bands, respectively.

D. RECEIVER SENSITIVITY

Figure 10 shows the BER performances as a function of ROP for the conventional multi-twin-SSB and the proposed ZGB multi-twin-SSB scheme after 50 km fiber downlink transmission at the OSNR of 35 dB. The guard band of the conventional scheme is set to 6 GHz while no guard band is

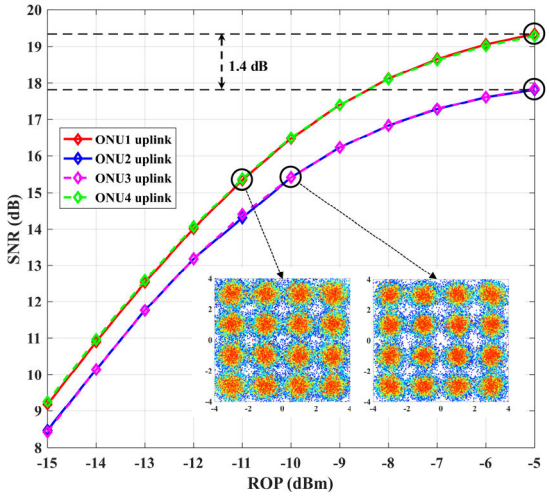

FIGURE 12. SNR performance versus ROP at the OSNR of 35 dB after 50 km uplink transmission.

used for the proposed scheme. For the conventional scheme, the required ROP at the 7% HD-FEC are about −8.8 dBm and −10.2 dBm for inner and outer sub-bands, respectively. While for the proposed scheme, the required ROP at the 7% HD-FEC are about −16.2 dBm and −17.8 dBm for the inner and outer sub-bands, respectively. The performance improvement for the proposed ZGB scheme is due to the optical carrier suppressed transmission and the heterodyne detection. It is observed that, for the ZGB multi-twin-SSB transmission, when the ROP is lower than −9 dBm, the performances of the inner sub-bands are worse than that of the outer sub-bands. This is because that the performance is mainly limited by the additive noise of the receiver when the ROP is insufficient and the minimum phase condition for KK algorithm is not satisfied. Nonetheless, the proposed ZGB multi-twin-SSB scheme can improve the receiver sensitivity by about 7.4 dB and 7.6 dB for the inner and out sub-bands, respectively.

E. THE UPLINK PERFORMANCE

Figure 11 shows the BER performance versus ROP at the OSNR of 35 dB after 50 km uplink transmission. The spectra of the upstream signals and the positions of ONU1-ONU4 are shown in the inset (a) of Fig. 11. Obviously, as the spectra of the downstream and the upstream signals do not overlap, the RB noise is effectively eliminated by the OBPF. Hence, the field of the upstream SSB signal can be well reconstructed by the KK algorithm. The typical constellations for ONU1 and ONU2 at the ROP of −5 dBm are shown in the inset (b) and (c) of Fig. 11. The required ROPs for the upstream signals at 7% HD-FEC are about −10 dBm and −11 dBm for the inner and outer sub-bands, respectively.

Figure 12 shows the SNR performance versus ROP at the OSNR of 35 dB after 50 km uplink transmission. The insets of Fig. 12 show the typical constellations of the ONU1 and ONU2 at the ROPs of −11 dBm and −10 dBm with the corresponding SNRs of 15.3 dB and 15.4 dB respectively. It is observed that since the impact of the SSBI on the inner

sub-bands is serious than the outer sub-bands, about 1.4 dB SNR penalty exist between the inner and outer sub-bands at the ROP of −5 dBm.

IV. CONCLUSION

In conclusion, a ZGB multi-twin-SSB system in single fiber bidirectional PON is proposed and investigated in this paper. A null point biased IQ modulator is applied at the downlink transmitter side to suppress the optical carrier and obtain a more linear modulation. An optical LO whose central frequency lays at the opposite edge of the undesired sideband is needed before detection. KK algorithm is adopted at the receiver side DSP to reduce the required CSPR as well as eliminate the SSBI induced by the square-law detection. Thanks for that, only a weak optical LO which extracted from the uplink optical source is needed for the downstream signal detection. Since the residual part of the unwanted sideband and the desired sideband are at the same side of the optical LO, the whole filtered signal can be regarded as an integrated SSB signal which makes it possible to be well reconstructed by KK algorithm after square-law detection. Therefore, no guard band is needed in the proposed scheme and the SE is theoretically improved. In addition, as the optical carrier is not transmitted with the desired signal, the proposed ZGB multi-twin-SSB scheme can significantly improve the receiver sensitivity and reduce the required OSNR. For the uplink transmission, a quadrature point biased single DDMZM is applied to modulate the SSB signal. The subsequent upstream and downstream signals locate at different sides of the optical carrier so their spectra do not overlap. Hence the RB noise is easily eliminated by the OBPF. The results show that, compared with the conventional multi-twin-SSB downlink transmission, the proposed ZGB multi-twin-SSB scheme can improve the SE by about 11%. The required OSNR and the required ROP at the 7% HD-FEC threshold can also be reduced by more than 15 dB and 7 dB respectively. For the uplink transmission, the required ROPs for the inner and outer sub-bands at 7% HD-FEC are about −10 dBm and −11 dBm, respectively. And the SNR to the corresponding ROPs for the inner and outer sub-bands are 15.4 dB and 15.3 dB, respectively. We believe that the proposed ZGB multi-twin-SSB system can play a role in the future single fiber bidirectional PON applications beyond this work.

REFERENCES

[1] D. Nesset, "NG-PON2 technology and standards," *J. Lightw. Technol.*, vol. 33, no. 5, pp. 1136–1143, Mar. 1, 2015.

[2] S. Ullah, R. Ullah, A. Khan, H. A. Khalid, Q. Zhang, Q. Tian, F. Khan, and X. Xin, "Optical multi-wavelength source for single feeder fiber using suppressed carrier in high capacity LR-WDM-PON," *IEEE Access*, vol. 6, pp. 70674–70684, 2018.

[3] J.-H. Hsu, M. Yu, F. Liu, C.-H. Lin, C.-T. Lin, L. Zhou, L. Fang, and C.-C. Wei, "On channel estimation schemes for APD-based DDM-OFDM-PONs under sub-Nyquist sampling," *Opt. Express*, vol. 26, no. 18, pp. 23808–23818, Sep. 2018.

[4] A. Shahpari, "Coherent access: A review," *J. Lightw. Technol.*, vol. 35, no. 4, pp. 1050–1058, Feb. 15, 2017.

[5] L. Jiang, B. Liu, Y. Mao, J. Ren, X. Xu, X. Wu, Y. Zhang, and L. Zhang, "Flexible filter bank multi-carriers PON based on two-dimensional multiple probabilistic shaping distribution," *IEEE Access*, vol. 7, pp. 1793–1799, 2019.

[6] M. Rannello, M. Artiglia, M. Presi, and E. Ciaramella, "10 Gb/s long-reach PON system based on directly modulated transmitters and simple polarization independent coherent receiver," *Opt. Express*, vol. 25, no. 15, pp. 17841–17846, Jul. 2017.

[7] X. Li, S. Zhou, F. Gao, M. Luo, Q. Yang, Q. Mo, Y. Yu, and S. Fu, "4 × 28 Gb/s PAM4 long-reach PON using low complexity nonlinear compensation," in *Proc. Opt. Fiber Commun. Conf. Exhib. (OFC)*, Los Angeles, CA, USA, 2017, Art. no. M3H.4.

[8] R. Ullah, L. Bo, S. Ullah, M. Yaya, F. Tian, M. K. Khan, and X. Xiangjun, "Flattened optical multicarrier generation technique for optical line terminal side in next generation WDM-PON supporting high data rate transmission," *IEEE Access*, vol. 6, pp. 6183–6193, 2018.

[9] G.-R. Lin, Y.-S. Liao, Y.-C. Chi, H.-C. Kuo, G.-C. Lin, H.-L. Wang, and Y.-J. Chen, "Long-cavity Fabry–Perot laser amplifier transmitter with enhanced injection-locking bandwidth for WDM-PON application," *J. Lightw. Technol.*, vol. 28, no. 20, pp. 2925–2932, Oct. 2010.

[10] G.-R. Lin, H.-L. Wang, G.-C. Lin, Y.-H. Huang, Y.-H. Lin, and T.-K. Cheng, "Comparison on injection-locked Fabry–Perot laser diode with front-facet reflectivity of 1% and 30% for optical data transmission in WDM-PON system," *J. Lightw. Technol.*, vol. 27, no. 14, pp. 2779–2785, Jul. 15, 2009.

[11] J.-M. Kang, San, Y.-Y. Won, J.-S. Lee, Y.-K. Oh, D.-H. Jang, and S.-K. Han, "A novel hybrid WDM/SCM-PON using reflective semiconductor optical amplifier," in *Proc. Int. Top. Meeting Microw. Photon.*, 2005, pp. 181–184.

[12] C. Kottke, J. Elbers, K. Habel, M. Eiselt, H. Griesser, J. von Hoyningen-Huene, and W. Rosenkranz, "Coherent SCM-WDM-PON system using OFDM or single carrier with SSB modulation and wavelength reuse," in *Proc. 39th Eur. Conf. Exhibit. Opt. Commun. (ECOC)*, 2013, pp. 1–3.

[13] H. H. Hao He, J. L. Jun Li, M. B. Meihua Bi, and W. H. W. Hu, "20-Gbps low cost WDM-OFDM-PON downstream transmission with tunable filter and linear APD module," *Chin. Opt. Lett.*, vol. 12, no. 4, pp. 040603–40607, 2014.

[14] C. Chen, W.-D. Zhong, and D. Wu, "Integration of variable-rate OWC with OFDM-PON for hybrid optical access based on adaptive envelope modulation," *Opt. Commun.*, vol. 381, pp. 10–17, Dec. 2016.

[15] M. I. Olmedo, T. Zuo, J. B. Jensen, Q. Zhong, X. Xu, S. Popov, and I. T. Monroy, "Multiband carrierless amplitude phase modulation for high capacity optical data links," *J. Lightw. Technol.*, vol. 32, no. 4, pp. 798–804, Feb. 15, 2014.

[16] C.-Y. Lin, Y.-C. Chi, C.-T. Tsai, H.-Y. Wang, and G.-R. Lin, "39-GHz millimeter-wave carrier generation in dual-mode colorless laser diode for OFDM-MMWoF transmission," *IEEE J. Sel. Topics Quantum Electron.*, vol. 21, no. 6, pp. 609–618, Nov. 2015.

[17] Y.-C. Chi, Y.-C. Li, H.-Y. Wang, P.-C. Peng, H.-H. Lu, and G.-R. Lin, "Optical 16-QAM-52-OFDM transmission at 4 Gbit/s by directly modulating a coherently injection-locked colorless laser diode," *Opt. Express*, vol. 20, no. 18, pp. 20071–20077, Aug. 2012.

[18] M. I. Olmedo, Z. Tianjian, J. B. Jensen, Z. Qiwen, X. Xu, and I. T. Monroy, "Towards 400GBASE 4-lane solution using direct detection of MultiCAP signal in 14 GHz bandwidth per lane," in *Proc. Opt. Fiber Commun. Conf. Exhib. (OFC)*, Anaheim, CA, USA, 2013, Art. no. PDP5C.10.

[19] J. Zhang, J. Yu, F. Li, N. Chi, Z. Dong, and X. Li, "11 × 5 × 9.3 Gb/s WDM-CAP-PON based on optical single-side band multi-level multi-band carrier-less amplitude and phase modulation with direct detection," *Opt. Express*, vol. 21, no. 16, pp. 18842–18848, Aug. 2013.

[20] J. Wei and E. Giacoumidis, "Multi-band CAP for next-generation optical access networks using 10-G optics," *J. Lightw. Technol.*, vol. 36, no. 2, pp. 551–559, Jan. 2018.

[21] Y. Zeng, Z. Dong, Y. Chen, X. Wu, H. He, J. You, and Q. Xiao, "A novel CAP-WDM-PON employing multi-band DFT-spread DMT signals based on optical Hilbert-transformed SSB modulation," *IEEE Access*, vol. 7, pp. 29397–29404, 2019.

[22] M. Zhu, J. Zhang, X. Yi, Y. Song, B. Xu, X. Li, X. Du, and K. Qiu, "Hilbert superposition and modified signal-to-signal beating interference cancellation for single side-band optical NPAM-4 direct-detection system," *Opt. Express*, vol. 25, no. 11, May 2017, Art. no. 12622.

[23] L. Zhang, T. Zuo, Y. Mao, Q. Zhang, E. Zhou, G. N. Liu, and X. Xu, "Beyond 100-Gb/s transmission over 80-km SMF using direct-detection SSB-DMT at C-band," *J. Lightw. Technol.*, vol. 34, no. 2, pp. 723–729, Jan. 15, 2016.

[24] X. Zhang, C. Zhang, C. Chen, W. Jin, and K. Qiu, "Non-optical carrier SSB-OFDM PONs with the improved receiver sensitivity and potential transmission nonlinearity tolerance," *IEEE Photon. J.*, vol. 9, no. 1, pp. 1–10, Feb. 2017.

[25] X. Zhang, C. Zhang, C. Chen, M. Zhu, W. Jin, and K. Qiu, "Bidirectional SSB modulation for Hybrid-PON with source-free optical network units," in *Proc. Asia Commun. Photon. Conf.*, Guangzhou, China, Nov. 2017, Art. no. Su2A.27.

[26] X. Zhang, C. Zhang, C. Chen, W. Jin, and K. Qiu, "All-optical VPN utilizing DSP-based digital orthogonal filters access for PONs," *Opt. Commun.*, vol. 413, pp. 347–352, Apr. 2018.

[27] A. Mecozzi, C. Antonelli, and M. Shtaif, "Kramers–Kronig coherent receiver," *Optica*, vol. 3, no. 11, p. 1220, 2016.

[28] X. Chen, C. Antonelli, S. Chandrasekhar, G. Raybon, A. Mecozzi, M. Shtaif, and P. Winzer, "Kramers–Kronig receivers for 100-km datacenter interconnects," *J. Lightw. Technol.*, vol. 36, no. 1, pp. 79–89, Jan. 1, 2018.

[29] C. Antonelli, A. Mecozzi, M. Shtaif, X. Chen, S. Chandrasekhar, and P. J. Winzer, "Polarization multiplexing with the kramers–kronig receiver," *J. Lightw. Technol.*, vol. 35, no. 24, pp. 5418–5424, Dec. 15, 2017.

[30] Z. Li, M. S. Erkilinc, K. Shi, E. Sillekens, L. Galdino, T. Xu, B. C. Thomsen, P. Bayvel, and R. I. Killey, "Digital linearization of direct-detection transceivers for spectrally efficient 100 Gb/s/λ WDM metro networking," *J. Lightw. Technol.*, vol. 36, no. 1, pp. 27–36, Jan. 1, 2018.

[31] X. Gao, B. Xu, Y. Cai, M. Zhu, J. Zhang, and K. Qiu, "QAM modulation with single DDMZM based on direct-detection and Kramers-Kronig scheme in long reach PON," *Opt. Fiber Technol.*, vol. 48, pp. 289–296, Mar. 2019.

[32] S. T. Le, K. Schuh, M. Chagnon, F. Buchali, R. Dischler, V. Aref, H. Buelow, and K. M. Engenhardt, "1.72-Tb/s virtual-carrier-assisted direct-detection transmission over 200 km," *J. Lightw. Technol.*, vol. 36, no. 6, pp. 1347–1353, Mar. 2018.

[33] L. Zhang, T. Zuo, Q. Zhang, E. Zhou, G. N. Liu, and X. Xu, "Transmission of 112-Gb/s+ DMT over 80-km SMF enabled by twin-SSB technique at 1550 nm," in *Proc. Eur. Conf. Opt. Commun. (ECOC)*, Sep. 2015, pp. 1–3.

[34] S. Fan, Q. Zhuge, Z. Xing, K. Zhang, T. M. Hoang, M. Morsy-Osman, M. Y. S. Sowailem, Y. Li, J. Wu, and D. V. Plant, "264 Gb/s twin-SSB-KK direct detection transmission enabled by MIMO processing," in *Proc. Opt. Fiber Commun. Conf. (OFC)*, San Diego, CA, USA, 2018, Art. no. W4E.5.

[35] S. Fan, Q. Zhuge, M. Y. S. Sowailem, M. Morsy-Osman, T. M. Hoang, F. Zhang, M. Qiu, Y. Li, J. Wu, and D. V. Plant, "Twin-SSB direct detection transmission over 80 km SSMF using Kramers–Kronig receiver," in *Proc. Eur. Conf. Opt. Commun. (ECOC)*, Sep. 2017, pp. 1–3.

[36] L. Zhang, T. Zuo, Q. Zhang, J. Zhou, E. Zhou, and G. N. Liu, "150-Gb/s DMT over 80-km SMF transmission based on spectrally efficient SSBI cancellation using guard-band twin-SSB technique," in *Proc. Eur. Conf. Opt. Commun. (ECOC)*, 2016, pp. 1–3.

[37] L. Zhang, T. Zuo, Q. Zhang, J. Zhou, E. Zhou, and G. N. Liu, "Single wavelength 248-Gb/s transmission over 80-km SMF based on twin-SSB-DMT and direct detection," in *Proc. Eur. Conf. Opt. Commun. (ECOC)*, 2016, pp. 1–3.

[38] G. N. Liu, L. Zhang, T. Zuo, and Q. Zhang, "IM/DD transmission techniques for emerging 5G fronthaul, DCI, and metro applications," *J. Lightw. Technol.*, vol. 36, no. 2, pp. 560–567, Jan. 15, 2018.

[39] Y. Zhu, "4 × 200 Gb/s twin-SSB Nyquist subcarrier modulation WDM transmission over 160 km SSMF with direct detection," in *Proc. Opt. Fiber Commun. Conf. Exhib. (OFC)*, San Diego, CA, USA, 2018, Art. no. W4E.5.

[40] M. Chen, M. Peng, H. Zhou, Z. Zheng, X. Tang, and L. Maivan, "Receiver sensitivity improvement in spectrally-efficient guard-band twin-SSB-OFDM using an optical IQ modulator," *Opt. Commun.*, vol. 405, pp. 259–264, Dec. 2017.

[41] S. Fan, Y. Li, Z. Xing, T. M. Hoang, M. Sowailem, M. Morsy-Osman, J. Wu, Q. Zhuge, and D. V. Plant, "Comparison of Kramer–Kronig receiver and one-stage SSBI mitigation algorithm in twin-SSB direct detection transmission systems enabled by MIMO processing," *Opt. Commun.*, vol. 434, pp. 75–79, Mar. 2019.

[42] Y. Zhu, X. Ruan, K. Zou, and F. Zhang, "Beyond 200G direct detection transmission with nyquist asymmetric twin-SSB signal at C-band," *J. Lightw. Technol.*, vol. 35, no. 17, pp. 3629–3636, Sep. 1, 2017.

[43] C. H. Wang, C. W. Chow, C. H. Yeh, C. L. Wu, S. Chi, and C. Lin, "Rayleigh noise mitigation using single-sideband modulation generated by a dual-parallel MZM for carrier distributed PON," *IEEE Photon. Technol. Lett.*, vol. 22, no. 11, pp. 820–822, Jun. 2010.

[44] D. Li, Q. Yu, L. Deng, L. Huo, S. Fu, M. Tang, M. Cheng, M. Zhang, and D. Liu, "Bidirectional long-reach PON using Kramers–Kronig-based receiver for Rayleigh backscattering noise and SSBI interference elimination," *Opt. Express*, vol. 26, no. 15, pp. 19020–19036, Jul. 2018.

[45] S. Amiralizadeh, A. T. Nguyen, C. S. Park, and L. A. Rusch, "Single-fiber lightwave centralized WDM-OFDMA-PON with colorless optical network units," *J. Opt. Commun. Netw.*, vol. 8, no. 4, p. 196, Apr. 2016.

[46] X. Gao, Y. Cai, B. Xu, X. Zhang, and K. Qiu, "Multi-twin-SSB modulation with direct detection based on Kramers–Kronig scheme for long-reach PON downstream," *Appl. Sci.*, vol. 9, no. 4, p. 748, Feb. 2019.

[47] Q. Zhang, N. Stojanovic, C. Xie, C. Prodaniuc, and P. Laskowski, "Transmission of single lane 128 Gbit/s PAM-4 signals over an 80 km SSMF link, enabled by DDMZM aided dispersion pre-compensation," *Opt. Express*, vol. 24, no. 21, pp. 24580–24591, Oct. 2016.

[48] W.-R. Peng, X. Wu, K.-M. Feng, V. R. Arbab, B. Shamee, J.-Y. Yang, L. C. Christen, A. E. Willner, and S. Chi, "Spectrally efficient direct-detected OFDM transmission employing an iterative estimation and cancellation technique," *Opt. Express*, vol. 17, no. 11, pp. 9099–9111, May 2009.

[49] W.-R. Peng, X. Wu, V. Arbab, K.-M. Feng, B. Shamee, L. Christen, J.-Y. Yang, A. Willner, and S. Chi, "Theoretical and experimental investigations of direct-detected RF-tone-assisted optical OFDM systems," *J. Lightw. Technol.*, vol. 27, no. 10, pp. 1332–1339, May 2009.

[50] Q. Zhou, J. He, S. Shen, R. Zhang, S. Yao, Y. Alfadhli, Y.-W. Chen, and G.-K. Chang, "Symmetric long-reach 16-QAM transmission using lite coherent receiver for next-generation optical access network," in *Proc. Opt. Fiber Commun. Conf. (OFC)*, San Diego, CA, USA, 2019, Art. no. Th2A.29.

[51] I. Fatadin, D. Ives, and S. J. Savory, "Laser linewidth tolerance for 16-QAM coherent optical systems using QPSK partitioning," *IEEE Photon. Technol. Lett.*, vol. 22, no. 9, pp. 631–633, May 2010.

[52] W. Shieh and K.-P. Ho, "Equalization-enhanced phase noise for coherent-detection systems using electronic digital signal processing," *Opt. Express*, vol. 16, no. 20, pp. 15718–15727, Sep. 2008.

[53] I. Fatadin, D. Ives, and S. J. Savory, "Carrier phase recovery for 16-QAM using QPSK partitioning and sliding window averaging," *IEEE Photon. Technol. Lett.*, vol. 26, no. 9, pp. 854–857, May 2014.

[54] R. A. Shafik, M. S. Rahman, and A. R. Islam, "On the extended relationships among EVM, BER and SNR as performance metrics," in *Proc. Int. Conf. Electr. Comput. Eng. (ICECE)*, 2006, pp. 408–411.

XIANG GAO received the M.S. degree in optical engineering from the University of Electronic Science and Technology of China, Chengdu, China, in 2014, where he is currently pursuing the Ph.D. degree in optical engineering. His research interests include advanced modulation/detection techniques for high data-rate optical communication systems, and optical access networks.

YUANCHENG CAI received the M.S. degree in optical engineering from the University of Electronic Science and Technology of China, Chengdu, China, in 2014, where he is currently pursuing the Ph.D. degree in optical engineering. His research interests include microwave photonics and optical communications.

BO XU received the B.Sc. degree from the Department of Electronic Science, Nankai University, Tianjin, China, in 1996, and the Ph.D. degree in electronic engineering from the Department of Electronic and Computer Engineering, University of Virginia, in 2003. From 2003 to 2004, he held a postdoctoral position in optical fiber communication systems with the University of Virginia. In June 2004, he joined in the Key Laboratory of Broadband Optical Fiber and Communication Network Technology, Ministry of Education, School of Communication and Information Engineering, University of Electronic Science and Technology of China (UESTC), Chengdu, China, where he is currently a Full Professor with the School of Information and Communication Engineering. His research interests include optical fiber communication systems, optical network, microwave optical fiber systems, and its application in wireless mobile.

FAITH KWAKU DEYNU received the M.S. degree in telecommunication engineering from the HAN University of Applied Sciences, The Netherlands, in 2011. He is currently pursuing the Ph.D. degree in information and communication engineering with the University of Electronic Science and Technology of China (UESTC), Chengdu, China. His research interests include IP multimedia subsystems, system engineering, and optical fiber communication systems.

KUN QIU received the M.S. and Ph.D. degrees from Tsinghua University, Beijing, China, in 1987 and 1990, respectively. In 1990, he joined the University of Electronic Science and Technology of China, where he was involved in the theories and technologies in optical fiber communications. From 1993 to 1994, he was a Visiting Scholar with the Institution of Optics, University of Rochester. From 2002 to 2006, he was the Director of the State Key Laboratory of the Broadband Optical Transmission and Communication Network. He has finished more than 20 important projects as a Research Team Leader. He has authored over 200 scientific articles and the book of *Optical Fiber Communication*. He received eight awards of science and technology progress from provinces or ministries. He is the Chair of the Chengdu Chapter of the IEEE Photonics Society.